

# Mineralogical investigations of the first package of the alternative buffer material test – I. Alteration of bentonites

S. KAUFHOLD<sup>1,\*</sup>, R. DOHRMANN<sup>1,2</sup>, T. SANDÉN<sup>3</sup>, P. SELLIN<sup>4</sup> AND D. SVENSSON<sup>4</sup>

<sup>1</sup> BGR, Bundesanstalt für Geowissenschaften und Rohstoffe, Stilleweg 2, D-30655 Hannover, Germany,

<sup>2</sup> LBEG, Landesamt für Bergbau, Energie und Geologie, Stilleweg 2, D-30655 Hannover, Germany,

<sup>3</sup> Clay Technology AB, IDEON Research Center, S-223 70 Lund, Sweden, and <sup>4</sup> SKB, Svensk Kärnbränslehantering AB, Stockholm, BOX 5864, S-102 40 Stockholm, Sweden

(Received 20 December 2012; revised 14 February 2013; Editor: Enver Murad)

**ABSTRACT:** Bentonite, which is envisaged as a promising engineered barrier material for the safe disposal of highly radioactive waste, was and is investigated in different large scale tests. The main focus was and is on the stability (or durability) of the bentonite. However, most countries concentrated on one or a few different bentonites only, regardless of the fact that bentonite performance in different applications is highly variable. Therefore, SKB (Svensk Kärnbränslehantering) set up the first large scale test which aimed at a direct comparison of different bentonites. This test was termed the ‘alternative buffer material test’ and considers eleven different clays which were either compacted (blocks) or put into cages to keep the material together. One so-called package consisted of thirty different blocks placed on top of each other. These blocks surrounded a heated iron tube 10 cm in diameter. Altogether three packages were installed in the underground test laboratory Äspö, Sweden. The first package was terminated 28 months after installation and the bentonite had been exposed for the maximum temperature (130°C) for about one year.

Almost all geochemical and mineralogical alterations of the different bentonites (apart from exchangeable cations) were restricted to the contact between iron and bentonite. The increase of the Fe<sub>2</sub>O<sub>3</sub> content was attributed to corrosion of the tube. However, the typical 7 or 14 Å smectite alteration product was not found. At the contact of one sample, siderite was precipitated. Some samples showed anhydrite and organic carbon accumulation and some showed dissolution of clinoptilolite and cristobalite. IR spectroscopy, XRD, and XRF data indicated the formation of trioctahedral minerals/domains in the case of some bentonites. Even more data has to be collected before unambiguous conclusions concerning both alteration mechanisms and bentonite differences can be drawn.

**KEYWORDS:** bentonite, HLRW disposal, radwaste, alternative buffer material test, smectite alteration, URL.

Bentonite is a candidate material for the encapsulation of radioactive waste in high-level radioactive waste (HLRW) repositories (e.g. Pusch, 1997; SKB,

2011). Its desired properties are large swelling pressure, which directly translates into sealing capacity, and radionuclide retention (at least of some radionuclides) by sorption. The required bentonite property is stability (or durability) under the expected conditions. One of the most comprehensive studies on HLRW bentonites, including requirements and desired properties, is provided by

\* E-mail: s.kaufhold@bgr.de

DOI: 10.1180/claymin.2013.048.2.04

Pusch (2002a, b) and SKB (2010). The term “HLRW bentonite” refers to bentonites which are planned to be used as geotechnical barrier material.

With respect to the stability of bentonites under the conditions expected, four scenarios have to be considered: (1) contact with possibly flowing hot brines, (2) dry periods, e.g. in the course of permafrost events, (3) contact with metal from canisters or construction elements in tunnels, and (4) contact with cements used as plugs. Laboratory experiments conducted under well-defined conditions may help identify the mechanisms of mineral transformation. Additional important results, however, can be derived from large- to real-scale tests. Accordingly, several countries are conducting different large- and/or real-scale tests commonly based on their current concept for HLRW disposal. Large-scale tests are larger than laboratory scale (>1 m), but do not resemble the real-scale test.

For more than a decade SKB has been conducting a set of large- and real-scale tests. One example is the so called “Long Term Test” (LOT), which consists of a heated central copper tube with a diameter of 10 cm enclosed by bentonite rings (10 cm) yielding a total diameter of 30 cm. In all these tests only MX-80 bentonite from Wyoming has been used. However, in 2006 the Alternative Buffer Material test (ABM) was launched in which eleven different clay materials were tested. In the present study this test is termed ABM. Most of the included clays are rich in montmorillonite while others are low or very low in swelling clay minerals. Both Na- and Ca-bentonite were included as well as mixtures, also with Mg and traces of K in the interlayer position. The main objectives of the project are to characterize the clays before and after the experiments and to identify any differences in behaviour or long term stability. Several international collaborators are investigating the clays and their geotechnical, chemical, mineralogical and microbiological properties and contents. This paper concerns the first package that was excavated in May 2009.

Probably because of their high temperature, the SKB experiments, as the LOT test mentioned above, revealed some processes which may take place. Analysing samples from the LOT test showed copper corrosion (including formation of a Cu corrosion product; a covellite-like phase) and dissolution/precipitation processes of gypsum. These or similar reactions were expected to also occur in the ABM experiment.

The aim of the present study is to investigate possible chemical and mineralogical changes, i.e. alteration of the swelling minerals and to collect relevant data to eventually draw conclusions with respect to the selection of an ideal HLRW bentonite.

## MATERIALS AND METHODS

The experimental setup, sampling for the present study, and temperature curves are shown in Fig. 1. Altogether three identical ABM packages were installed in the Äspö Hard Rock Laboratory. Different running times of the three packages were thought to provide kinetic information on possible mineral reactions. The first package was terminated 28 months after installation and the bentonite had been exposed for the maximum temperature (130°C) for about one year. Results obtained on the 1-year blocks are presented in the present paper.

The large-scale test ABM is based on the Swedish KBS-3 concept. ABM started at Äspö Hard Rock Laboratory during November 2006 (Svensson *et al.*, 2007, 2010, 2011) with a metal canister surrounded by clay positioned in crystalline bedrock at approximately 500 m depth. The differences to the large-scale test are mainly the smaller scale, the heat source (thermal energy supplied by a heater), instrumentation such as sensors, initial water content (this is varied in each block, depending on which material used), and that the canister is made of iron instead of copper. The experiment consisted of three packages in three separate bore holes with a diameter of 30 cm and a depth of 3 m. The packages were moistened by natural water from cracks in the rock and optionally also artificially from the installed wetting system. Eleven different clays included as compacted rings penetrated by the heater were positioned on top of each other. To allow testing of bentonite pellets (granulate; MX-80 and 30 mass% sand), cages were constructed of black steel covered with a fibre cloth and filled with the pellets. The cages were constructed to keep the pellets in place during installation, to minimize the disturbance on water transport and to hold the weight of the upper buffer blocks. The level of monitoring was kept at a minimum in order not to disturb the experiment. Two of the packages were heated from the start and the third package was heated after water saturation was complete. The clays used were diverse in

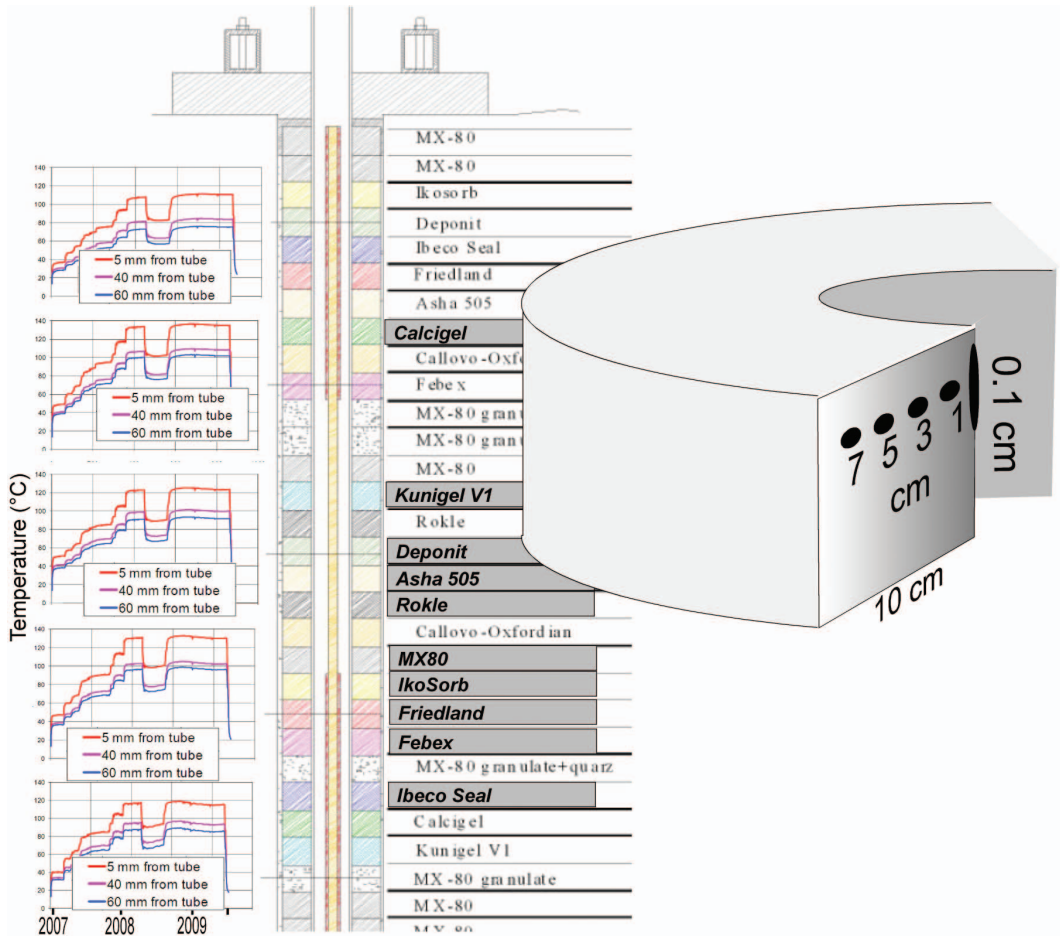


FIG. 1. Experimental set-up, temperature curves (source SKB), and sampling. The '0.1 cm sample' was produced by scraping off the surface with a sharp knife.

quality, for example with iron content ranging from below 2 to almost 14 wt.%  $\text{Fe}_2\text{O}_3$ .

At least one block of each bentonite from the hottest parts was selected and sampled. Each block was sampled at five different distances from the contact with the metal tube (Fig. 1). The sample labelled '0.1 cm' was collected by scraping off the surface with a sharp knife.

The samples were dried at  $60^\circ\text{C}$  and ground by a mortar mill. The chemical composition was determined by XRF and C/S-LECO-analysis. For XRF analysis of powdered samples, a PANalytical Axios and a PW2400 spectrometer were used. Samples were prepared by mixing with a flux material (lithium metaborate Spectroflux, Flux No.

100A, Alfa Aesar) and melting into glass beads. The beads were analyzed by wavelength-dispersive X-ray fluorescence spectrometry (WD-XRF). To determine loss on ignition (LOI), 1000 mg of sample material were heated to  $1030^\circ\text{C}$  for 10 min. The organic carbon (OC) content was measured with a LECO CS-444-Analysator after carbonate dissolution by treating the samples several times at  $80^\circ\text{C}$  with HCl until no further gas evolution could be observed. Samples of 170–180 mg of the dried material were used to measure the total carbon (TIC) content. The TIC was calculated by the difference of TIC-TOC. The samples were heated in the device to  $1800\text{--}2000^\circ\text{C}$  under an oxygen atmosphere and the evolved  $\text{CO}_2$  was detected by

	JNB ABM 'Kunigel V1' Bentonite #17	CAN ABM Deponit Ca N Bentonite #15	ROK ABM 'RAWRA' = ROK???? #13	CAL ABM 'Caligel' Bentonite #23	IBE ABM 'IBECO Seal' Bentonite #6
<i>Block</i>	<i>"metallic" crust, hard, a little rusty but thin</i>	<i>blue until 1 cm depths, direct contact bluegreen</i>	<i>thin black crust at contact, pristine clay underneath</i>	<i>a thick (1mm) black layer</i>	<i>black layer at contact with white spots, smells rotten</i>
					
1 mm	JNB 0	CAN 0	ROK 0	CAL 0	IBE 0
1 cm	JNB 1	CAN 1	ROK 1	CAL 1	IBE 1
3 cm	JNB 2	CAN 2	ROK 2	CAL 2	IBE 2
5 cm	JNB 3	CAN 3	ROK 3	CAL 3	IBE 3
7 cm	JNB 4	CAN 4	ROK 4	CAL 4	IBE 4
					IBE 0-1 white (1mg)
	LOT ABM 'MX 80' Bentonite #11	ASH ABM 'Asha 505' Bentonite #14	FRI ABM 'Friedland' Clay #9	FEB ABM 'Febex' Bentonite #8	IKO ABM 'Ikosorb' Bentonite #10
<i>Block</i>	<i>total sample dark, contact is brittle</i>	<i>no colour change at contact, smells as a disinfectant</i>	<i>pieces fell apart, contact very hard</i>	<i>blue seems, contact brittle, thick, black</i>	<i>very hard dark corrosion products at contact</i>
					
1 mm	LOT 0	ASH 0	FRI 0	FEB 0	IKO 0
1 cm	LOT 1	ASH 1	FRI 1	FEB 1	IKO 1
3 cm	LOT 2	ASH 2	FRI 2	FEB 2	IKO 2
5 cm	LOT 3	ASH 3	FRI 3	FEB 3	IKO 3
7 cm	LOT 4	ASH 4	FRI 4	FEB 4	IKO 4

Fig. 2. Photographs of the blocks before sampling, and sample list.

an infrared detector. C/S values presented in the manuscript may be referred to as "LECO results". The error of the LECO values in the present study is <0.1 wt.%.

For mineralogical analysis, XRD, IR, and DTA-MS were used. XRD patterns were recorded using a PANalytical X'Pert PRO MPD  $\theta$ - $\theta$  diffractometer (Cu-K $\alpha$  radiation generated at 40 kV and 30 mA), equipped with a variable divergence slit (20 mm irradiated length), primary and secondary sollers, Scientific X'Celerator detector (active length 0.59°) and a sample changer (sample diameter 28 mm). The samples were scanned from 2° to 85° 2 $\theta$  with a step size of 0.0167° 2 $\theta$  and a measuring time of

10 s per step. For specimen preparation, the top-loading technique was used. A different setup and side-loading preparation was used for the  $d_{060}$  patterns only: here the wavelength (Co), the detector (proportional counter), and measuring conditions such as step size (0.02°) and time (5 s/step) were changed. For mid (MIR) and far (FIR) infrared spectra, the KBr pellet technique (1 mg sample/200 mg KBr) was applied. Spectra were collected on a Thermo Nicolet Nexus FTIR spectrometer (MIR beam splitter KBr, detector DTGS TEC; FIR beam splitter solid substrate, detector DTGS PE). The resolution was adjusted to 2 cm<sup>-1</sup>. Thermoanalytical investigations were

performed using a Netzsch 409 PC thermobalance equipped with a DSC/TG sample holder linked to a Pfeiffer ThermoStar quadrupole mass spectrometer (MS). 100 mg of powdered material previously equilibrated at 53% relative humidity (RH) were heated from 25–1000°C at a rate of 10 K/min.

## RESULTS AND DISCUSSION

### *Iron–bentonite interactions*

The photographs (Fig. 2) indicate that different reactions occurred at the iron–bentonite interface. Iron corrosion is known to lead to smectite alteration with berthierine-like minerals or chlorites as products (e.g. Wersin & Mettler, 2006). Therefore, samples were investigated with respect to Fe distribution and identification of possible alteration products. Furthermore, dissolved Fe may have been precipitated, which is considered a corrosion product in contrast to a possible smectite alteration product.

The most significant Fe accumulation was observed at the contact surface of the JNB block (Fig. 3). The  $\text{Fe}_2\text{O}_3$  content increased from 2 wt.% to almost 18 wt.%. For the latter sample, siderite precipitation was confirmed by XRD, IR, and DTA-MS (Fig. 4).

Samples CAN, ROK, and ASH showed nearly no Fe accumulation. In all others,  $\text{Fe}_2\text{O}_3$  increased by 2–4 wt.%. Siderite, however, was not confirmed in

either contact sample. The Fe, therefore, was believed to be in a separate phase or in the smectite interlayers. Typical corrosion products generally are Fe-oxyhydroxides. While most published smectite alteration products are 7 or 14 Å phases (Mosser-Ruck *et al.*, 2010), none of which were detected in the present study. Exchangeable Fe could not be detected in CEC analyses. XRD with ethylene glycol saturation did not show an increased intensity at 7 Å which would be indicative for the presence of an alteration product. The absence of such neo-formed minerals was unexpected because the macroscopic appearance and the brittle character of the contact of some samples, e.g. FEB or IKO (compare Fig. 2), led to the assumption that chlorite or related non-swelling (7 Å) minerals had been formed.

### *Sulfur distribution*

At the contact along the iron–bentonite interface brines might migrate, at least initially. This may have caused accumulation of phases other than Fe minerals. The LOT test demonstrated the redistribution of gypsum which, as a minor MX80 component, was evenly distributed before the heating period (Karnland *et al.*, 2009). After the heating period, gypsum was dissolved both at the inner and outer parts and had accumulated in the centre of the blocks. In the Prototype Project an S accumulation at the contact was also observed

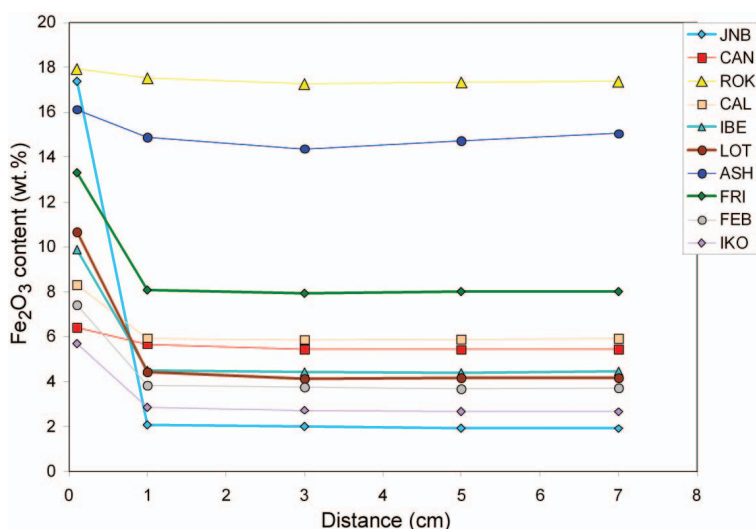


FIG. 3. Content of  $\text{Fe}_2\text{O}_3$  depending on the distance to the heater (sample list in Fig. 2).

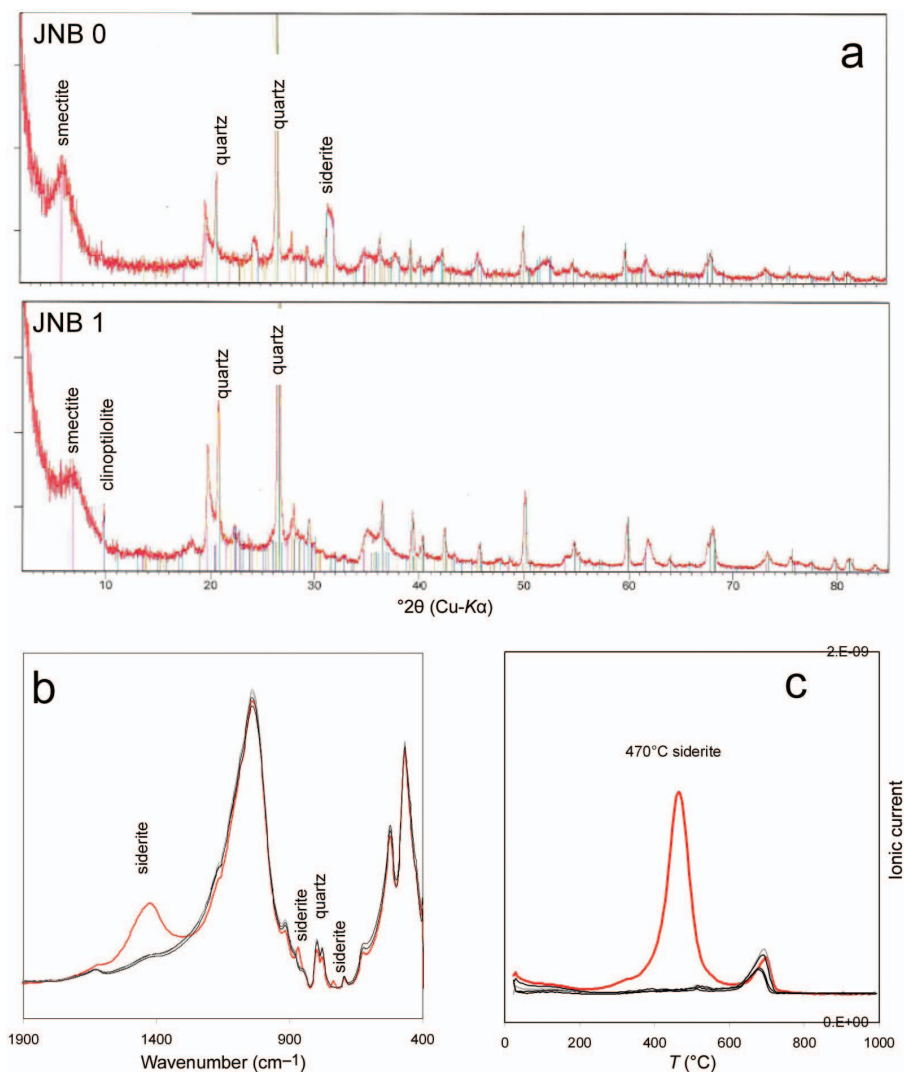


FIG. 4. Identification of siderite in the contact sample (0.1 cm, red curves) of JNB by (a) XRD, (b) IR, and (c) DTA-MS.

(Dueck *et al.* 2011). Accordingly, LECO analysis was carried out to investigate similar dissolution/precipitation processes.

A clear redistribution, as observed for the gypsum of the LOT project (Karlund *et al.*, 2009), was not found (Fig. 5). This process obviously was less important in the ABM test than in the LOT test, which operated with a Cu tube and only one bentonite (MX80). The reasons are not yet understood. The most significant change was observed for sample FEB (Fig. 5), in which S increased from less than 0.1 wt.% to almost 1 wt.%.

This can be explained by the precipitation of anhydrite, which was detected by XRD and DTA-MS (sulfate decomposition starts at 900 $^{\circ}\text{C}$ , Fig. 6c). IR spectroscopy revealed a band at 680  $\text{cm}^{-1}$ , which could correspond to anhydrite, but could also indicate trioctahedral minerals such as saponite (Fig. 6b). Because of the absence of the characteristic saponite stretching band at 3680  $\text{cm}^{-1}$ , the 680  $\text{cm}^{-1}$  band is assumed to result from anhydrite, which was also detected in sample IBE by analysing one of the small white spots with IR (Figs 2 and 7).

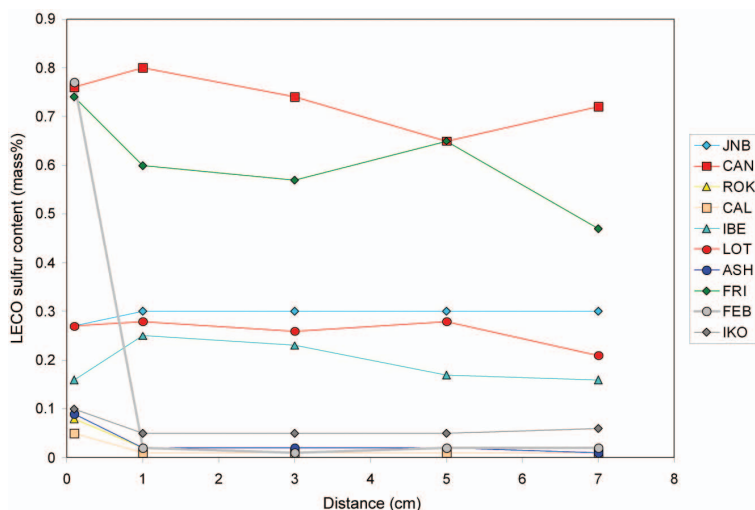


FIG. 5. Distribution of sulfur concentrations from LECO analysis (sample list in Fig. 2).

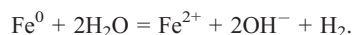
### Carbon distribution

The distribution of inorganic and organic carbon is shown in Fig. 8. Only sample JNB showed a significant accumulation of inorganic carbon at the contact, which is probably related to the Fe corrosion because of siderite formation (Fig. 4). In contrast, almost all samples showed a significant increase of the organic carbon content, which indicates that organic carbon was transported along the iron–bentonite interface. The most significant increase was observed for sample ROK. IR spectra (Fig. 9) show the aliphatic stretching and deformation bands (symmetrical and asymmetrical vibrations according to Yule *et al.*, 2000). DTA-MS analysis indicates the organic matter to consist of a mixture of easily (LER) and more difficultly (HER) oxidizable organics (Friedrich *et al.*, 1996). The remaining question concerns the source of the organic matter. Prior to the experiment the tubes were coated with a thin layer of the lubricant ‘Molykote®BR2 plus’, which is a mixture of waxes, oil, graphite, molybdenite and Zn dialkyl dithiophosphate. Based on characteristic band and peak ratios, IR and DTA can characterize the source of the organic matter. The C-H stretching bands of the pure lubricant and the organic-rich ROK surface appear to be similar (Fig. 9a), whereas the C-H deformation band ratios appear to be different. This is caused by the shoulder of the Si-O stretching vibration. All contact samples with high organic carbon contents show the same ratio of DTA peaks, i.e. the

LER/HER ratio. The DTA-MS<sub>CO2</sub> curve of the pure lubricant was similar but not identical. The peak ratio 380/490 of the lubricant was significantly larger. Therefore no unambiguous conclusion could be drawn and further research is needed.

### Silicate dissolution

Under laboratory conditions, the only water-soluble components of bentonites are carbonates and gypsum. However, hydrothermal conditions, as expected in a HLRW repository and as present in the ABM test, significantly shift the solubility of minerals. In addition, iron corrosion can lead to high pH values, further promoting silicate dissolution:



The identification of possibly dissolved minerals was one of the important questions to be answered in the ABM project.

Figure 4 shows that clinoptilolite could not be determined by XRD in the JNB sample of the contact. All other JNB samples contained XRD-detectable clinoptilolite which indicates that clinoptilolite was dissolved at the contact. One may speculate whether this is related to local pH changes or simply because of the elevated temperature. JNB was the only sample containing a zeolite mineral.

From Fig. 6 it can be concluded that cristobalite was dissolved at the contact. In fact, all other FEB

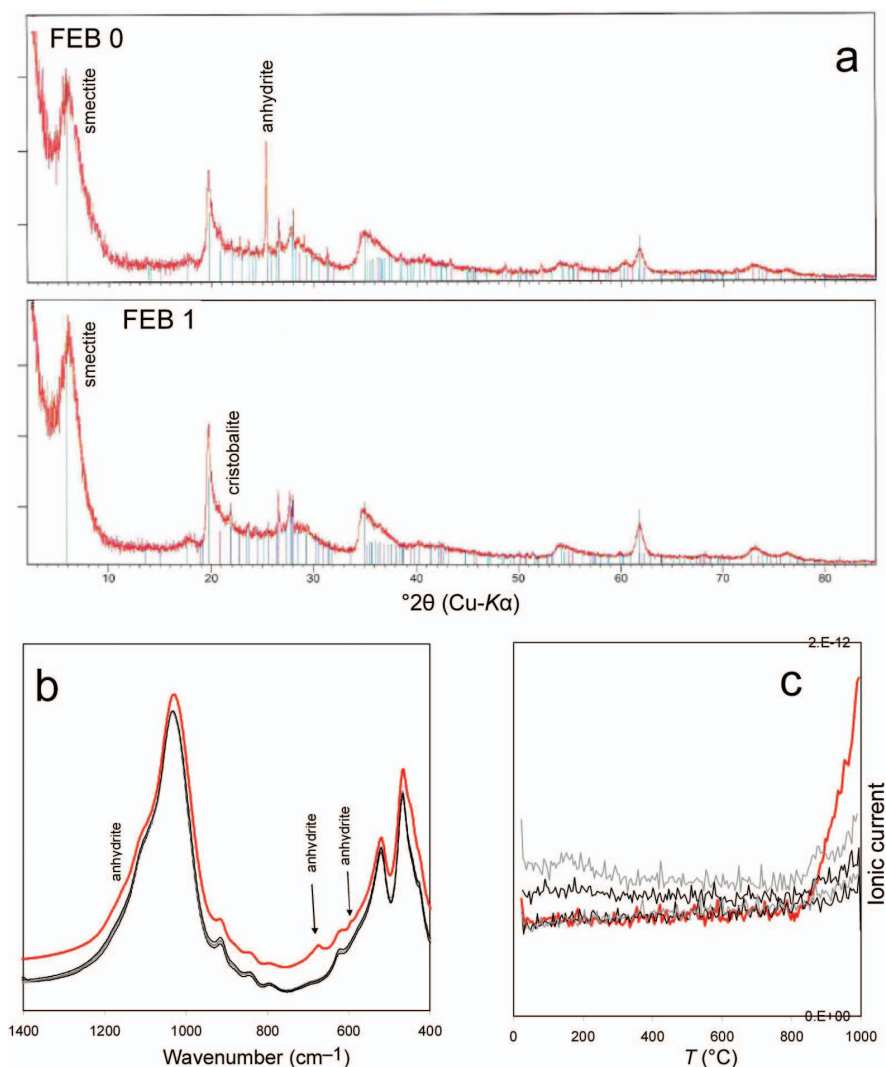


FIG. 6. Identification of anhydrite in the contact sample (0.1 cm, red curves) of FEB by XRD (a), IR (b), and DTA-MS (c).

samples contained XRD-detectable cristobalite, which indicates that cristobalite was dissolved at the contact with sample FEB. Interestingly the other two samples initially containing cristobalite (LOT and IKO) also lacked the cristobalite at the contact (Fig. 10). This cristobalite dissolution indicates a high pH at the interface.

Further evidence for dissolution and possible precipitation is provided by IR spectroscopy. In samples CAL and IKO a weak but significant intensity was observed at 3740 cm $^{-1}$  (Fig. 11),

which corresponds to 'free silica' derived either from smectite alteration (dissolution, heat-treatment; Madejova *et al.*, 2009) or from the precipitation of silica which flowed along the iron–bentonite interface. This band was observed for diatomites (Yuan *et al.*, 2004), molecular sieves (Luan & Fournier, 2005) and many siliceous compounds, and is assigned to isolated, terminal silanol groups. Such groups exist in weakly crystallized SiO $_2$  polymorphs and structurally degraded smectites, and the band is assigned to a Si-OH stretching vibration.

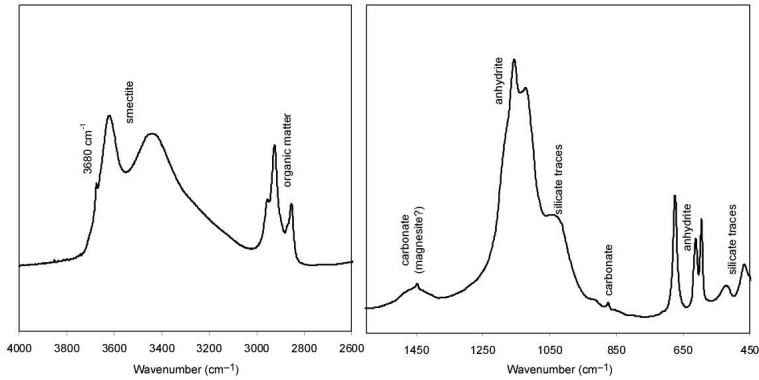


FIG. 7. IR spectrum of one of the white spots (this sample was labelled IBE-0-IR; 1 mg), containing mainly anhydrite with some smectite, organic matter and carbonate.

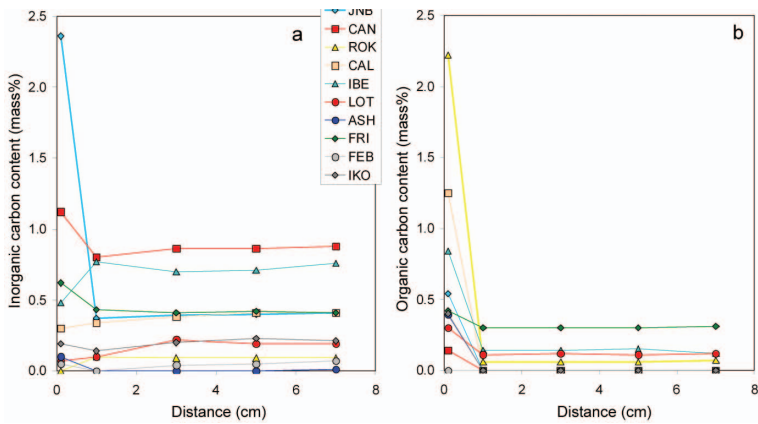


FIG. 8. Distribution of inorganic (a) and organic (b) carbon (sample list in Fig. 2).

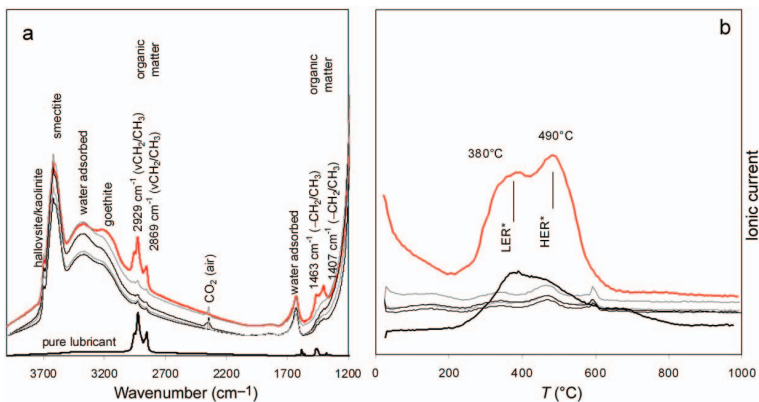


FIG. 9. IR spectrum (9a, left) and DTA-MS<sub>CO<sub>2</sub></sub> (9b, right) curves of the ROK samples (contact sample 0.1 cm: red curves) which showed the most significant increase of organic carbon (terminology according to Friedrich *et al.*, 1996) and of the pure lubricant (2 wt.% added to pure smectite).

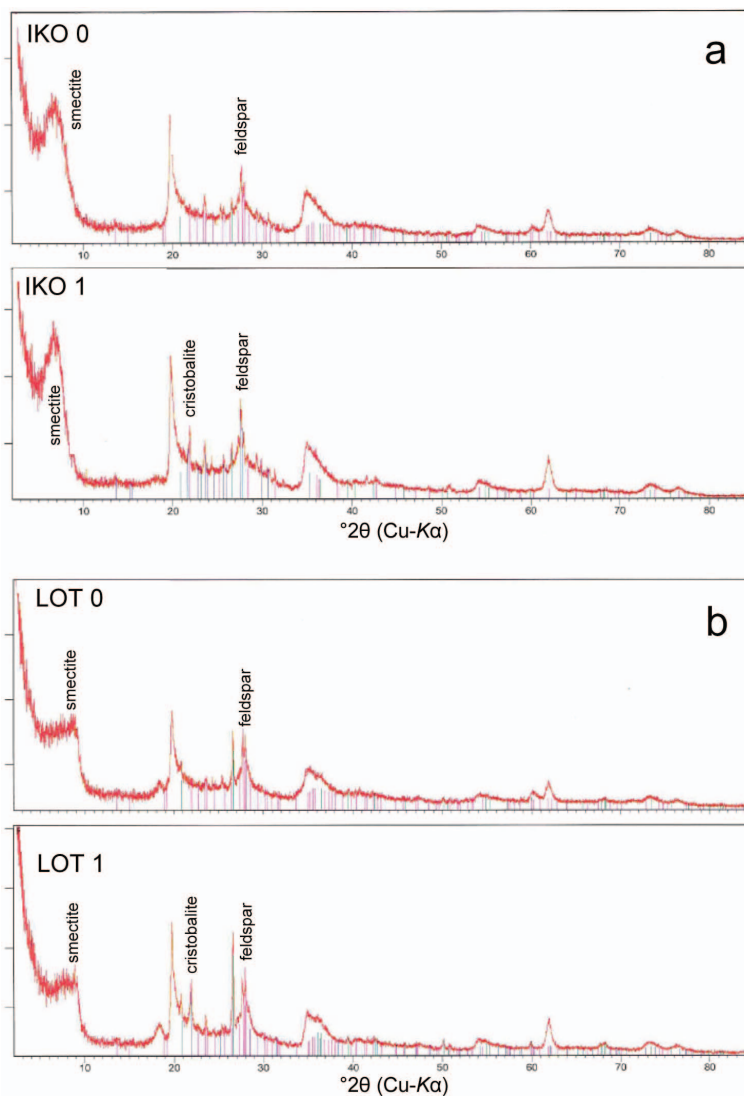


FIG. 10. XRD patterns of samples IKO (a) and LOT (=MX80) (b) showing the missing cristobalite reflection in the sample of the contact area.

### *Smectite alteration*

Results of the LOT project showed that the Mg content increased at and near the contact (Karnland *et al.*, 2009). This was observed previously by Fernandez & Villar (2010) and may be related to the better solubility of Mg compared to the other structural cations of smectite. In other words, Mg is dissolved first (incongruently). In the magnetic fraction of the Mg-enriched LOT bentonite, some layered double hydroxides were found, which could be an explanation for the increased Mg content.

This result, however, has to be validated. Therefore, the ABM bentonites were investigated with respect to the Mg increase and possible structural changes. Interestingly, most of the ABM bentonites showed an Mg increase at the contact (Fig. 12). Notably, this Mg increase does not correspond to exchangeable Mg. The exchangeable cations are discussed in the second part of this publication (Dohrmann *et al.*, 2013).

One indication of the mechanism behind the Mg increase is provided by infrared spectroscopy. Some

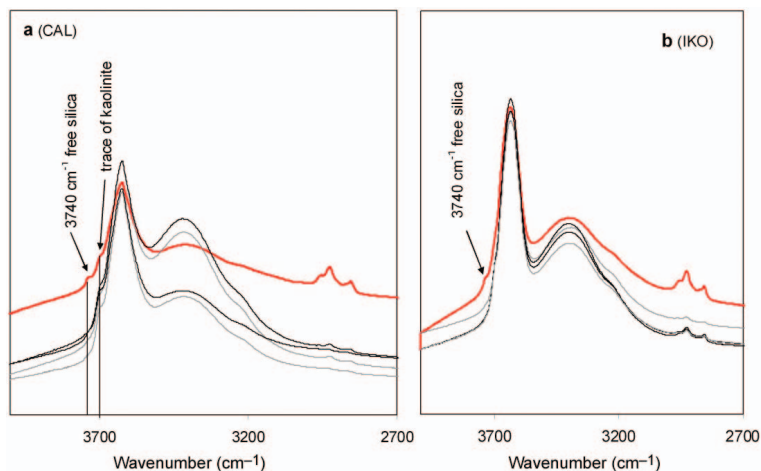


FIG. 11. OH-stretching regions of samples CAL (a) and IKO (b), both showing significant intensity at  $3740\text{ cm}^{-1}$  for the contact sample (red curves) related to free silica.

samples showed a slight increase of intensity at  $680\text{ cm}^{-1}$ , which can be attributed to anhydrite or saponite (a trioctahedral 2:1 mineral). In the case of sample CAN, no S increase at the contact was found both by LECO and DTA-MS. Based on data from the latter, the S content of this sample is entirely in the form of sulfide. Since DTA-MS is able to detect traces of sulfate and none was found in sample CAN, the  $680\text{ cm}^{-1}$  intensity is tentatively attributed to trioctahedral minerals or domains, possibly saponite but hydrocalcite and vermiculite (as

ferrous saponite) are also conceivable. The same band was observed in sample LOT, again with no sulfate accumulation according to LECO and DTA-MS (Fig. 13b). The increase of the  $680\text{ cm}^{-1}$  intensity in samples FRI and FEB cannot be interpreted unambiguously because of the presence of anhydrite. Sample IKO (not shown in Fig. 13) also showed an increased intensity at  $680\text{ cm}^{-1}$ .

The  $d_{060}$  XRD reflection supports the concept of the formation of trioctahedral minerals and/or domains. Those samples with large increase of the

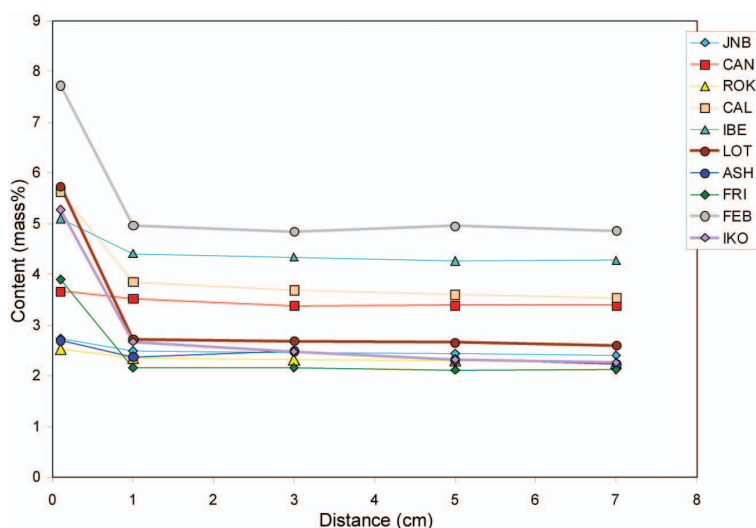


FIG. 12. MgO content of the ABM bentonites (sample list in Fig. 2).

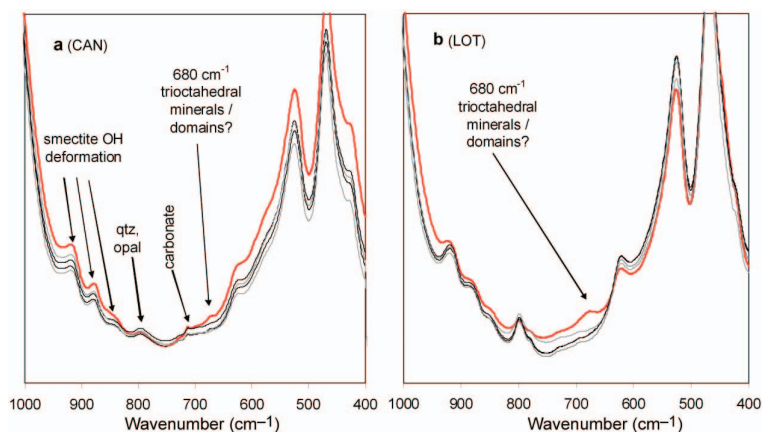


FIG. 13. IR spectra of samples from the contact (red curves): CAN (a) and LOT (b) (as examples) showing increased  $680\text{ cm}^{-1}$  intensities which cannot be attributed to precipitation of sulfates.

$680\text{ cm}^{-1}$  band all showed an increased XRD intensity at  $1.54\text{ \AA}$ , corresponding to trioctahedral minerals (samples FEB, LOT, IKO; Fig. 14). For sample CAN, a slight increase of the  $680\text{ cm}^{-1}$  intensity was observed, but the XRD pattern showed no changes. In Fig. 14, sample ROK is plotted as reference.

## SUMMARY AND CONCLUSIONS

Almost all geochemical and mineralogical alterations of the different bentonites from the first package of the ABM test were restricted to the contact between iron and bentonite. Most of the samples showed an accumulation of Fe. In the bentonite with the largest  $\text{Fe}_2\text{O}_3$  accumulation, siderite was identified as a newly formed phase. In the other samples with an increase of the  $\text{Fe}_2\text{O}_3$  content ranging from 2–4 wt.%, no separate Fe phase or interlayer Fe were found. Gypsum redistribution, as detected in the LOT experiment (LOT had similar boundary condition, but only one bentonite, MX80, and a Cu-heater were used; Karnland *et al.*, 2009), was not observed. Two samples showed anhydrite precipitation at the contact, which indicates that S was transported along the iron–bentonite interface. An increase of the inorganic carbon content was only found for the sample with siderite precipitation, and hence is possibly linked to corrosion processes. On the other hand, all samples showed organic carbon accumulation at the iron–bentonite interface. IR and DTA-MS characteristics may be used to identify the source of organic matter, i.e. whether it was

derived from the production of the blocks or if it was natural organic matter from an unknown source. DTA and IR analyses of the organic matter and the lubricant used during installation of the experiment did not provide a clear picture. More research is required to (i) identify the source of the organic material and (ii) identify possible effects of the lubricant on the smectite.

Apart from the precipitation of relatively soluble phases such as carbonates or gypsum/anhydrite, some silicates were dissolved at the contact. Clinoptilolite and cristobalite were dissolved, indicating alkaline conditions at the interface which could have been caused by the corrosion. IR spectroscopy revealed the presence of low-crystalline silica phases or surface groups.

The most relevant factor, however, is the stability of smectites. Some samples showed a slight increase of IR intensity at  $680\text{ cm}^{-1}$ , either corresponding to sulfate precipitation or formation of trioctahedral minerals and/or domains, e.g. from saponite, vermiculite or even hydrotalcite. At least for the two sulfate-free samples showing increased  $680\text{ cm}^{-1}$  intensity, the formation of trioctahedral minerals and/or domains is strongly indicated. This view was supported by XRD. Considering the  $d_{060}$  reflection suggests that trioctahedral minerals formed. This would explain the increased Mg content at the contact. The observed mineralogical changes are summarized in Table 1.

The present study shows that different bentonites will perform differently under real HLRW repository conditions after a short time of approximately one year. However, the performance of the different

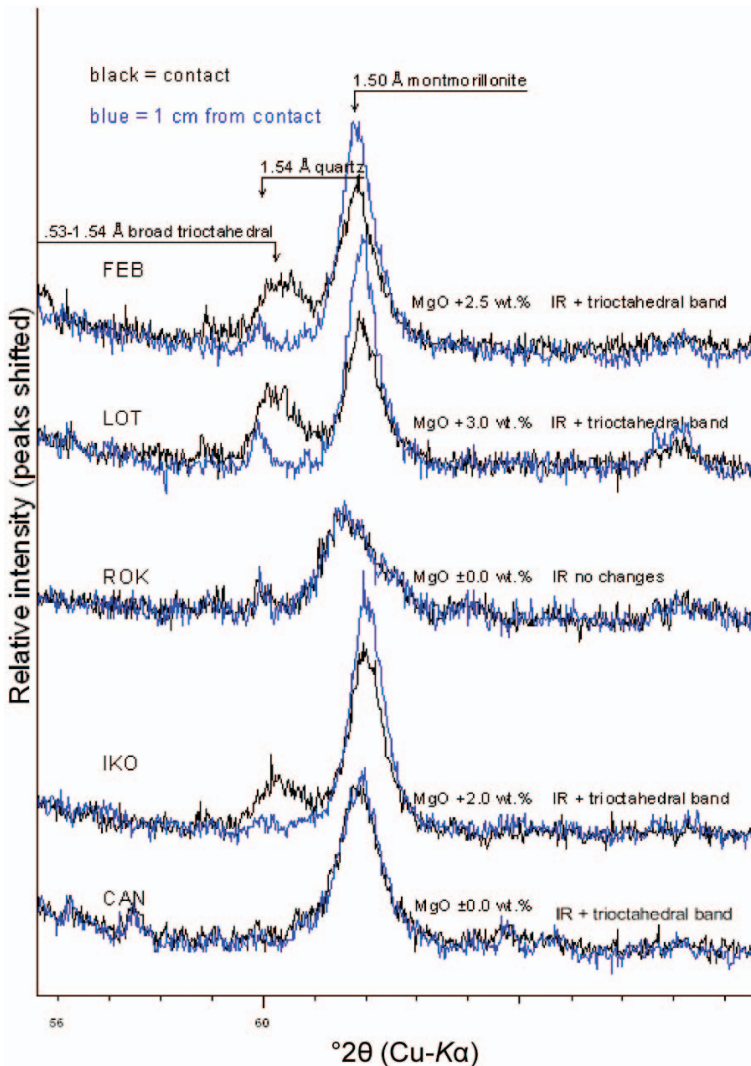


FIG. 14. XRD  $d_{060}$  reflection of selected samples.

bentonites cannot be assessed based on the data generated in this project, because of the hydraulic and electrical short-cuts between the blocks. Such a setup can be regarded as unrealistic for the final concept, but it offers the possibility to study vastly different bentonites. The investigation of the second package of the ABM test is expected to be particularly interesting with respect to the possible identification of the (trioctahedral) Mg phase and the corrosion/alteration products near the contact. The much longer reaction time is believed to increase the concentration of these phases, which will facilitate phase analysis. Finally, one could

speculate about the mechanism leading to the different alterations that were observed. However, comparing different large scale tests proved that the observed alterations (e.g. gypsum redistribution in the LOT) may be less significant than one would deduce from considering one experiment only. Therefore, the present study focused on summarizing the different observations, which at this point in the research is more reasonable than to conclusively speculate on mechanisms. In some years or decades, we expect the comparison of a set of experiments to lead to a deeper understanding of the (possibly linked) processes.

TABLE 1. Summary of observed reactions/changes of the different bentonite blocks.

	JNB ABM	CAN ABM	ROK ABM	CAL ABM	IBE ABM	LOT ABM	ASH ABM	FRI ABM	FEB ABM	IKO ABM
	'Kunigel V1' Bentonite Japan #17	'Deponit Ca N' Bentonite Milos, Greece #15	"RAWRA" Bentonite Czech Republic #13	'Calcigel' Bentonite Bayern #23	'IBECO Seal' Bentonite Georgia #6	'MX 80' Bentonite Wyoming #11	'Asha 505' Bentonite India #14	'Friedland' Clay Friedland, D. #9	'Febex' Bentonite Almeria, Spain #8	'Ikosorb' Bentonite Morocco #10
Fe-accumulation	++ sid.	–	–	+–	+–	+–	–	+–	+–	+–
XRD <sub>EG</sub>	full swell- ability, no 7 Å	full swellability, no 7 Å	full swell- ability, no 7 Å	full swell- ability, no 7 Å	full swellabil- ity, no 7 Å	full swell- ability, no 7 Å	full swell- ability, no 7 Å	full swell- ability, no 7 Å	full swell- ability, no 7 Å	full swell- ability, no 7 Å
XRD <sub>060</sub> trioctahedral?						+			+	+
C <sub>inorg</sub> accumulation	+									
C <sub>org</sub> accumulation	+–		+	+–	+–		+			+
SO <sub>4</sub> -accumulation					spots				+ anhyd	
Mineral dissolution	+ clinop						+ crist		+ crist	+ crist
680 cm <sup>-1</sup> IR band		+					+	+ anhyd?	+ anhyd	+
3740 cm <sup>-1</sup> IR band		+–		+			+–			+

The colours indicate whether the clay showed some changes or not. Hence the clay in a column with only brown colour would not be suitable for HLRW disposal. clinop: clinoptilolite; crist: cristobalite; anhyd: anhydrite

## REFERENCES

- Dohrmann R., Olsson S., Kaufhold S. & Sellin P. (2013) Mineralogical investigations of the alternative buffer material field test – II. Exchangeable cation population rearrangement. *Clay Minerals*, **48**, 215–233.
- Dueck A., Johannesson L.-E., Kristensson O., Olsson S. & Sjöland A. (2011) Hydro-mechanical and chemical-mineralogical analyses of the bentonite buffer from a full-scale field experiment simulating a high-level waste repository. *Clays and Clay Minerals*, **59**, 595–607.
- Fernández A.M. & Villar M.V. (2010) Geochemical behaviour of a bentonite barrier in the laboratory after up to 8 years of heating and hydration. *Applied Geochemistry*, **25**, 809–824.
- Friedrich A., Grunewald K., Klinnert S. & Bechmann W. (1996) Thermogravimetric and differential thermal analytical investigations on sewage farm soils. *Journal of Thermal Analysis and Calorimetry*, **46**, 1589–1597.
- Karland O., Olsson S., Dueck A., Birgersson M., Nilsson U., Hernan-Håkansson T., Pedersen K., Nilsson S., Eriksen T.E. & Rosborg B. (2009) Long term test of buffer material at the Äspö Hard Rock Laboratory, LOT project, Final report on the A2 test parcel. *SKB Technical Report TR-09-29*.
- Luan Z. & Fournier J.A. (2005) *In situ* FTIR spectroscopic investigation of active sites and adsorbate interactions in mesoporous aluminosilicate SBA-15 molecular sieves. *Microporous and Mesoporous Materials*, **79**, 235–240.
- Madejová J., Pentrák M., Pálková H. & Komadel P. (2009) Near-infrared spectroscopy: a powerful tool in studies of acid-treated clay minerals. *Vibrational Spectroscopy*, **49**, 211–218.
- Mosser-Ruck R., Cathelineau M., Guillaume D., Charpentier D., Rousset D., Barres O. & Michau N. (2010) Effects of temperature, pH, and iron/clay and liquid/clay ratios on experimental conversion of dioctahedral smectite to berthierine, chlorite, vermiculite, or saponite. *Clays and Clay Minerals*, **58**, 280–291.
- Pusch R. (1997) Deep disposal of radioactive waste. *Schriftenreihe Angewandte Geowissenschaften*, **1**, 85–96.
- Pusch R. (2002a) The buffer and backfill handbook part 1 – Definitions, basic relationships, and laboratory methods. *SKB Technical Report TR 02-20*.
- Pusch R. (2002b) The buffer and backfill handbook part 2 – Materials and techniques. *SKB Technical Report TR 02-12*.
- SKB (2010) Buffer, backfill and closure process report for the safety assessment SR-Site. SKB TR-10-47, Svensk Kärnbränslehantering AB.
- SKB (2011) Long-term safety for the final repository for spent nuclear fuel at Forsmark. Main report of the SR-Site project. SKB TR-11-01, Svensk Kärnbränslehantering AB.
- Svensson D., Eng A. & Sellin P. (2007) Alternative buffer material experiment. Conference abstract, 3rd International meeting, *Clays in Natural and Engineered Barriers for Radioactive Waste Confinement*. September 17–18, Lille, France.
- Svensson D., Sandén T., Kaufhold S. & Sellin P. (2010) Alternative buffer material experiment – experimental concept and progress. Conference abstract, 4th International meeting, *Clays in Natural & Engineered Barriers for Radioactive Waste Confinement*. March 29 – April 1, Nantes, France.
- Svensson, D., Sandén, T., Olsson, S., Dueck, A., Eriksson, S., Jägerwall, S. & Hansen, S. (2011) Alternative buffer material Status of the ongoing laboratory investigation of reference materials and test package 1. - SKB report TR-11-06.
- Wersin P. & Mettler S. (2006) Workshop on Fe-clay interactions in repository environments, a joint initiative by ANDRA, SKB and Nagra. Arbeitsbericht NAB 06-15.
- Yuan P., Wu D.Q., He H.P. & Lin Z.Y. (2004) The hydroxyl species and acid sites on diatomite surface: a combined IR and Raman study. *Applied Surface Science*, **227**, 30–39.
- Yule B.L., Roberts S. & Marshall J.E.A. (2000) The thermal evolution of sporopollenin. *Organic Geochemistry*, **31**, 859–870.